Biochemical and Biophysical Research Communications 417 (2012) 421–426

Contents lists available at SciVerse ScienceDirect

Biochemical and Biophysical Research Communications

journal homepage: www.elsevier.com/locate/ybbrc

Structural insight into the role of *Streptococcus parasanguinis* Fap1 within oral biofilm formation

James A. Garnett [a], Peter J. Simpson [a], Jonathan Taylor [a], Stefi V. Benjamin [a], Camille Tagliaferri [a], Ernesto Cota [a], Yi-Ywan M. Chen [b], Hui Wu [c], Stephen Matthews [a,*]

[a] Department of Biological Sciences, Centre for Structural Biology, Imperial College London, South Kensington, London SW7 2AZ, UK
[b] Department of Microbiology & Immunology, and Research Center for Pathogenic Bacteria, Chang Gung University, Tao-Yuan, Taiwan
[c] Department of Pediatric Dentistry, University of Alabama at Birmingham, School of Dentistry, Birmingham, AL 35294, USA

ARTICLE INFO

Article history:
Received 17 November 2011
Available online 7 December 2011

Keywords:
Fimbriae
Biofilm
Adhesion
Dental plaque
Streptococci
Serine-rich repeat

ABSTRACT

The fimbriae-associated protein 1 (Fap1) is a major adhesin of *Streptococcus parasanguinis*, a primary colonizer of the oral cavity that plays an important role in the formation of dental plaque. Fap1 is an extracellular adhesive surface fibre belonging to the serine-rich repeat protein (SRRP) family, which plays a central role in the pathogenesis of streptococci and staphylococci. The N-terminal adhesive region of Fap1 (Fap1-NR) is composed of two domains (Fap1-NR$_\alpha$ and Fap1-NR$_\beta$) and is projected away from the bacterial surface via the extensive serine-rich repeat region, for adhesion to the salivary pellicle. The adhesive properties of Fap1 are modulated through a pH switch in which a reduction in pH results in a rearrangement between the Fap1-NR$_\alpha$ and Fap1-NR$_\beta$ domains, which assists in the survival of *S. parasanguinis* in acidic environments. We have solved the structure of Fap1-NR$_\alpha$ at pH 5.0 at 3.0 Å resolution and reveal how subtle rearrangements of the 3-helix bundle combined with a change in electrostatic potential mediates 'opening' and activation of the adhesive region. Further, we show that pH-dependent changes are critical for biofilm formation and present an atomic model for the inter-Fap1-NR interactions which have been assigned an important role in the biofilm formation.

1. Introduction

Streptococcus parasanguinis, a commensal Gram-positive bacterium, is a primary coloniser of the human oral cavity and is involved in the development of dental plaque [1] and infective endocarditis [2–6]. Following adhesion to the oral surface, along with other oral streptococci, *S. parasanguinis* acts as a foundation upon which other bacterial species adhere, with the subsequent formation of an oral biofilm known as dental plaque [7]. Biofilms are complex structures, formed in specific stages and initiated by the attachment of bacteria to abiotic or biological surfaces [8]. This is followed by the development of an extrapolysaccharide matrix within microcolonies composed of a diverse population of commensal and pathogenic species, where access to a rich supply of nutrients and communication within these environments promotes a highly stable multicellular structure.

This ability of *S. parasanguinis* to bind to the oral cavity and also to other bacteria is attributed to the presence of long peritrichous fimbrial structures on the cell surface. One such fibre is composed of fimbria-associated protein 1 (Fap1), which is essential for fimbrial biogenesis, adhesion and biofilm formation. Glycan-specific antibodies raised against Fap1 inhibit the binding of *S. parasanguinis* FW213to an *in vitro* tooth model composed of saliva-coated hydroxyapatite (SHA) [9–13]. Fap1 is a ~200 kDa extracellular glycoprotein which has been characterized based on sequence and structural analysis [10,13]. The N-terminus contains a signal peptide which is cleaved during export, followed by a very short unique sequence, a minor serine-rich repeat (SRR) region, a much larger unique non-repeat region (Fap1-NR), an extensive SRR region and a C-terminal LPxTG cell wall anchor sequence (Fig. 1A). SRR glycoproteins belong to a growing number of bacterial adhesins which play an important role in pathogenesis and biofilm formation [12] and Fap1 is a model system to study this family. The SRRs of Fap1 are composed of S(V/I/E) dipeptide repeats which are O-glycosylated through the serine residues and serve to protect this extended, supercoiled region from degradation, whilst projecting the Fap1-NR domain away from the bacterial surface [13,14].

Fap1-NR is composed of two domains connected by a 27 amino acid linker; a three helix bundle (Fap1-NR$_\alpha$) at the N-terminus, followed by a predominantly β-sheet domain (Fap1-NR$_\beta$). These

* Corresponding author. Fax: +44 20 7594 3057.
E-mail address: s.j.matthews@imperial.ac.uk (S. Matthews).

0006-291X/$ - see front matter © 2011 Elsevier Inc. All rights reserved.
doi:10.1016/j.bbrc.2011.11.131

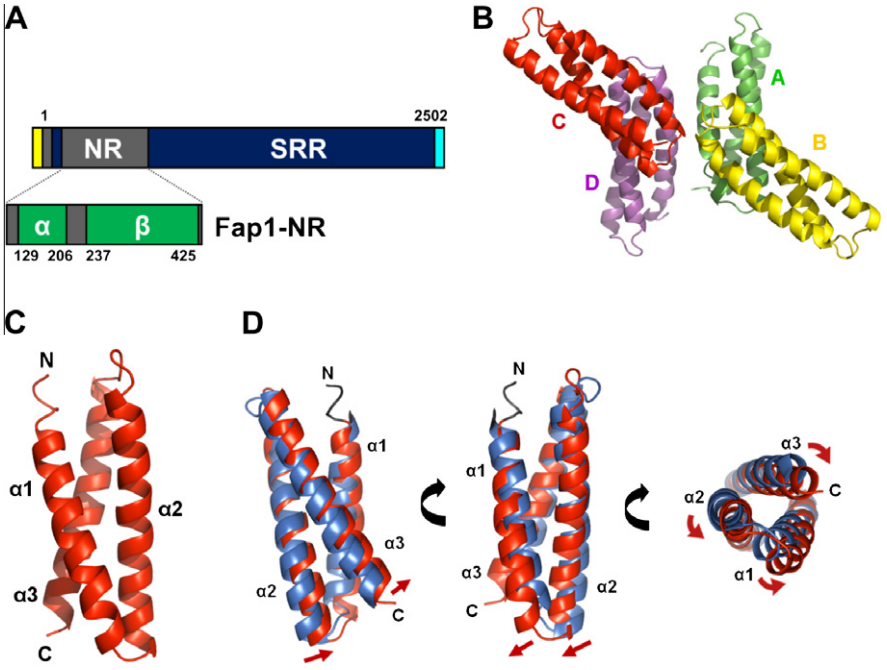

Fig. 1. Crystal structure and pH induced changes within Fap1-NR_α at pH 5.0. (A) Schematic representation of Fap1 with residue numbering shown for the mature protein. Signal peptide is yellow, serine-rich repeats (SRR) are blue, the unique non-repeat (NR) regions are grey and the cell anchor sequence is cyan. The major-NR repeat region (Fap1-NR) has been expanded and Fap1-NR_α and Fap1-NR_β are coloured green. (B) Asymmetric unit of Fap1-NR_α with chains coloured green (chain A), yellow (chain B), red (chain C) and magenta (chain D). (C) Single molecule of Fap1-NR_α with the three helices numbered and the N- and C-termini labelled. (D) Overlay of Fap1-NR_α at pH 5.0 (red) and 8.0 (blue) superimposed on residues at the N-terminal pole which display little variation in chemical shift in relation to changes in pH [14]. Those residues where there is no chemical shift change data available are coloured grey. (For interpretation of the references to colour in this figure legend, the reader is referred to the web version of this article.)

structures have been determined by solution state nuclear magnetic resonance (NMR) spectroscopy and X-ray crystallography, respectively, at pH 8.0 [14]. Using the *in vitro* tooth model, Fap1 has been shown to bind in a pH-dependent manner to SHA and further these adhesive properties have been attributed to the Fap1-NR region. Small angle X-ray scattering (SAXS) was used to map the low resolution envelope of Fap1-NR and revealed that at pH 8.0 the two domains adopt a boomerang appearance, which upon a reduction in pH move apart to open up the structure. In this 'adhesive state', under acidic conditions, the binding face becomes accessible and allows access to the host ligand. It has also been observed in EM images of cell-surface anchored Fap1 molecules at pH 5.0, that these adhesive tips have an increased tendency to come together in a very specific manner and this has been associated with a function in inter-Fap1 mediated biofilm interactions. Furthermore, NMR pH titrations of recombinant Fap1-NR clearly show that any pH-induced conformational changes can be solely ascribed to changes within the helical domain (Fap1 NR_α).

Survival within the oral cavity is achieved through adapting to a fluctuating environment including, for example changes in nutrient availability, pH and oxygen levels. Fermentation of sugars in the oral cavity regularly leads to a reduction in plaque pH below 5.0 in less than 3 min [15]. Many oral bacteria, such as *Streptococcus mutans*, have evolved systems to sense and change their physiology in order to survive in these acidic niches, known as the acid tolerance response [16–18]. *S. paransanguinis*, however, cannot endure these conditions and survives through shutting down its metabolism [18]. Fap1 presents an extracellular tool to allow *S. paransanguinis* to remain within these biofilms whilst in a state of 'metabolic sleep'. Here we have solved the crystal structure of Fap1-NR_α at pH 5.0 and herein describe how acidification leads to the activation of Fap1 and in addition present an atomic model for the inter-Fap1-NR interactions which have been assigned an important role in biofilm formation.

2. Materials and methods

2.1. Crystal structure determination and refinement

Crystals were obtained and data collected as previously described [14,19]. Data were processed using MOSFLM [20] and scaled with SCALA [21]. Phases were determined by molecular replacement with MOLREP [22] with the 'pseudo translational symmetry' option on, using the NMR structure of Fap1-NR_α [14] as the search model. Initial maps were subject to solvent flattening, 4-fold NCS averaging and histogram matching with PARROT [23] and automated model building was implemented using BUCANEER [24]. Refinement was carried out with REFMAC [25] using automated local NCS refinement, map sharpening and jelly body refinement, with 5% of the reflections omitted for cross-validation. Manual model building was carried out in COOT [26] and validated with MOLPROBITY [27]. Processing and refinement statistics for the final model can be found in Table 1.

2.2. Docking of Fap1-NR_α into the SAXS envelope at pH 5.0

The Fap1-NR_β crystal structure had previously been docked within the SAXS envelopes at pH 5.0 and 8.0, along with the NMR structure of Fap1-NR_α at pH 8.0 [14]. The SAXS maps were aligned via the β-domain and then the crystal structure of Fap1-NR_α was superimposed onto the NMR structure. This was then manually translated and rotated into the electron density map at pH 5.0.

2.3. T_1/T_2 experiments

^{15}N-labelled Fap1-NR_α was purified as described [14]. 1D envelope experiments on ^{15}N-labelled Fap1-NR_α in 50 mM $NaPO_4$ pH 5.0, 50 mM NaCl, 10% (v/v) D_2O were used to calculate T_1 and T_2

Table 1
Data collection statistics.

Crystal parameters	
Space group	$P4_13_12$
Cell dimensions	$a = b = 121.89$, $c = 117.98$
Data collection	
Beamline	SLS X06DA (PXIII)
Wavelength (Å)	0.939
Resolution (Å)	3.0–37.43 (3.0–3.16)
Unique observations	17284 (2502)
R_{sym}	0.08 (0.39)
$\langle I\rangle/\sigma I$	6.2 (1.9)
Completeness (%)	94.9 (95.9)
Redundancy	4.5 (4.4)
Refinement	
R_{work}/R_{free} (%)	22.3/24.2
Number of protein residues	351
Number of ligands/ions	1 glucose
Rmsd stereochemistry	
Bond lengths (Å)	0.011
Bond angles (°)	1.462
Ramachandran analysis	
Residues in outlier regions	0
Residues in favoured regions	93%
Residues in allowed regions	100%

Numbers in parentheses refer to the outermost resolution shell.
$R_{sym} = \sum|I - \langle I\rangle|/\sum I$ where I is the integrated intensity of a given reflection and $\langle I\rangle$ is the mean intensity of multiple corresponding symmetry-related reflections.
$R_{work} = \sum||F_o| - |F_c||/\sum F_o$ where F_o and F_c are the observed and calculated structure factors respectively.
$R_{free} = R_{work}$ calculated using ~5% random data excluded from the refinement.
rmsd stereochemistry is the deviation from ideal values.
Ramachandran analysis was carried out using *Molprobity* [27].

values at 298 K at different Fap1-NR$_\alpha$ concentrations: 200, 150, 100 and 50 μM. Average ^{15}N T_1 and T_2 relaxation rates were estimated by measuring the change in intensity of signals in the amide region above 8.8 ppm (i.e. to ensure unstructured residues were excluded) with varying T_1 or T_2 relaxation periods.

2.4. S. parasanguinis FW213 biofilm assay

The level of biofilm formation was assessed by the modified method of O'Toole and Kolter [28]. Overnight cultures of wild-type *S. parasanguinis* were diluted at 1:100 in fresh TH medium supplemented with 0, 20, 40, and 80 mM KPO_4 to achieve pH 5.3, 6.2, 6.6 and 7.0 respectively, and 200 μl of the diluted cultures was inoculated into wells of a non-tissue culture-treated polystyrene flat-bottom 96-well microtiter plate. Wells filled with only growth media were included as negative controls. Plates were incubated and treated as described before [13]. Biofilm formation was quantified by measuring absorbance of the dissolved crystal violet staining of bacteria attached to the surfaces at 562 nm with a VersaMax microplate reader (Molecular Devices).

2.5. Protein data bank accession number

The coordinates and structure factors of Fap1-NR$_\alpha$ have been deposited in the RCSB with accession codes 3RGU.

3. Results

3.1. Overall structure of Fap1-NR$_\alpha$ at pH 5.0

Fap1-NR$_\alpha$ was crystallized in 0.9 M K/Na PO_4 pH 5.0 [19] and belongs to the tetragonal space group $P4_32_12$. The structure was determined by molecular replacement at 3.0 Å using the NMR structure of Fap1-NR$_\alpha$ at pH 8.0 (pdb: 2kub) [14] as the search model. Due to the presence of pseudo translational symmetry, phase determination was not straightforward, although exploitation of this non-crystallographic relationship allowed the identification of four molecules in the asymmetric unit, with a very high solvent content of ~68% (Table 1 and Supplementary Fig. 1). The vector encoded N-terminal His_6 tags and Lys117-Gln123 (chains A and D), Lys117-Asp124 (chains B and C), Gly212-Ser231 (chains A and B) and Pro210-Ser231 (chains C and D) were disordered and not visible in the electron density maps. The final model includes 346 residues (Asp124-Asn211 chain A; Ser125-Asn211 chain B; Ser125-Asn209 chain C; Asp124-Asn209 chain D), 4 water molecules and 1 molecule of glucose (Fig. 1B) and chains A and D and chains B and C are related by the translational vector (0.5,0.469,0.5) (Supplementary Fig. 2). The four structures are essentially identical with an average rmsd of 0.18 Å (Supplementary Fig. 3) and as with the NMR structure at pH 8.0, under acidic conditions Fap1-NR$_\alpha$ is composed of a tightly packed three helix bundle (Fig. 1C).

3.2. Comparison between Fap1-NR$_\alpha$ at pH 5.0 and 8.0

We undertook a detailed analysis of the different structures of Fap1-NR$_\alpha$ to ascertain an atomic model for the effects of pH change on the global architecture of the non-repeat region. The NMR and crystal structures were superimposed giving an overall rmsd of 0.95 Å (Supplementary Fig. 4) between pH 5.0 and 8.0. Although it is evident that subtle variations exist between the two, it was not obvious how this related to function and so the structures were superimposed using residues which had previously displayed less dramatic variation in chemical shift with relation to changes in pH [14]. This lead to a more perceptible conformation change which coincides with the published titrations (Fig. 1D). Here, there is a subtle twisting of the C-terminal pole of Fap1-NR$_\alpha$ displacing the helices by ~2.5 Å. Furthermore, comparison of the isolated helices, independent of the intact structures, show that they are in essence identical (Supplementary Fig. 5), which supports the idea that changes in pH result in a delicate rearrangement of these helices with respect to one another. We began our interpretation of these rearrangements within Fap1-NR$_\alpha$ through analysing the hydrogen bond interactions between the three helices. There is, however, no clear and consistent pattern which indicates that the formation of salt bridges within Fap1-NR$_\alpha$ plays any role in the activation of the non-repeat adhesive region (Supplementary Table 1).

3.3. Electrostatic activation of Fap1-NR

We next turned our attention to the electrostatic potential of the domain under acidic and alkali conditions (Fig. 2A). When viewed along the length of the helices there are no dramatic shifts in charge caused by a change in pH, although the flexible N-terminus does show some variation in conformation. There is though a much more important reorganization at the C-terminal pole of Fap1-NR$_\alpha$ (Fig. 2B). At pH 8.0 the face is rather flat with patches of negative charge, whilst at pH 5.0 this charge becomes localized about a deep pocket sitting in the tri-helical interface. This can be attributed to the residues Asp152 and Glu154 which are positioned on the α1−α2 loop and it has been demonstrated in a number of other macromolecules that when buried acidic residues are clustered in close proximity, this has the effect of substantially raising the p*K*a of the side chain carboxylate groups [29–32]. Hence under alkali conditions these residues will be deprotonated whilst at pH 5.0 they may be fully protonated. Examination of the Fap1-NR$_\beta$ N-terminal pole, which lies adjacent to the α-domain in the non-repeat region, shows a highly complementary surface to Fap1-NR$_\alpha$ at pH 5.0. Arg368 protrudes straight out and is well positioned to

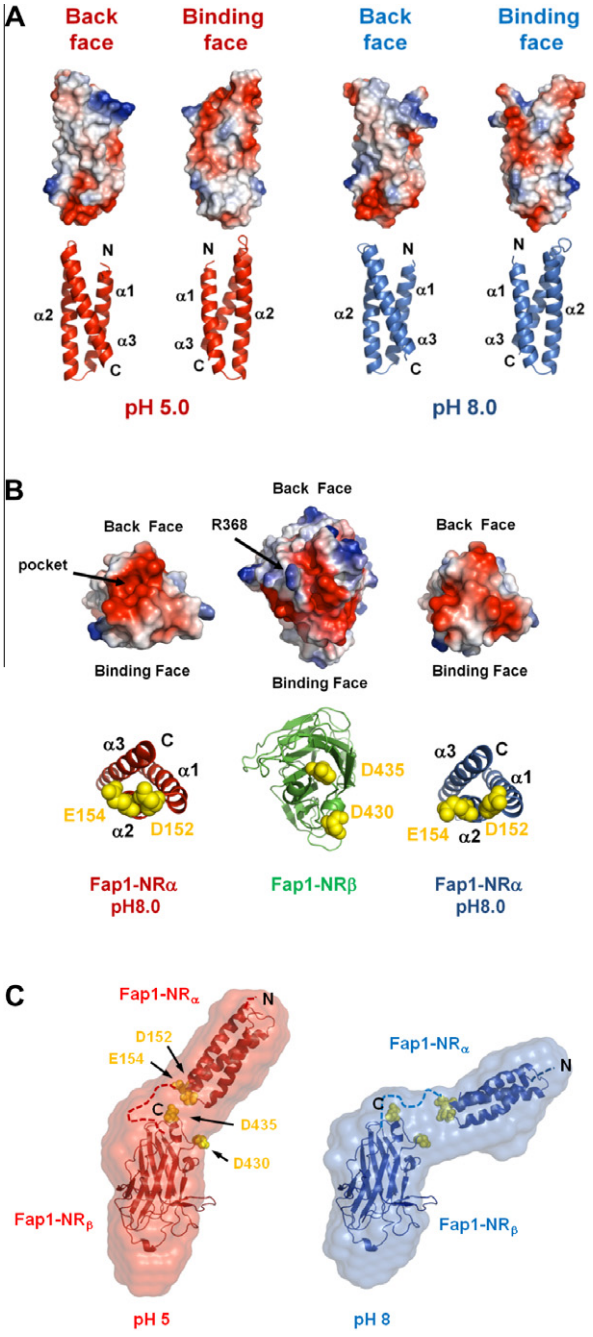

Fig. 2. Electrostatic activation of Fap1-NR. (A) Electrostatic surface potential of Fap1-NR$_\alpha$ at pH 5.0 and 8.0 shown from both sides. Cartoon is shown below for orientation. (B) Electrostatic potential of the inter domain surfaces of Fap1-NR$_\alpha$ at pH 5.0 and 8.0 and Fap1-NR$_\beta$ with cartoons displayed below for reference. The N-terminal pole of Fap1-NR$_\beta$ has a run of negative charge running along the centre towards the host binding face. Arg368 is positioned towards the centre of the face pointing directly out towards what would be Fap1-NR$_\alpha$, along with Asp430 and Asp435. At pH 8.0 the Fap1-NR$_\alpha$ C-terminal pole is rather flat and shows patches of negative charge and displays Asp152 and Glu154 on its surface. Under acidic conditions, the negative charge is localized towards a deep pocket which could accommodate Arg368. (C) SAXS electron density envelopes of Fap1-NR [14] at pH 5.0 (red) and 8.0 (blue) with the structures of Fap1-NR$_\beta$ and Fap1-NR$_\alpha$ at the respective pH docked into the maps. The inter domain linker is shown as dashed lines and residues Asp152 and Glu154 (Fap1-NR$_\alpha$) and Asp435 (Fap1-NR$_\beta$) have been coloured yellow and shown as spheres. (For interpretation of the references to colour in this figure legend, the reader is referred to the web version of this article.)

fill the negative pocket of the adjacent domain and further, residues Asp430 and Asp435 displayed on this face would be ideal candidates to form inter-domain salt bridges.

Using the published SAXS electron density maps [14], we were able to dock Fap1-NR$_\alpha$ into the envelope at pH 5.0 as we had done previously with the NMR structure (Fig. 2C). It is striking that under alkali conditions there will be substantial electrostatic repulsion between Asp152/Glu154 and Asp430/Asp435, whilst under acidic conditions this charge may be neutralized through the formation of one or more salt bridges across the domain interface. The mechanism of pH induced activation of Fap1 thus appears to be mediated via electrostatic effects between the α- and β-domains, with the correct formation of the active binding site groove between the two, likely determined by the insertion of Arg368 within the three-helices of Fap1-NR$_\alpha$.

3.4. Modelling biofilm interactions

Under acidic conditions Fap1 molecules aggregate much more readily via their tips [14] and further, when preparing Fap1-NR$_\alpha$ reagent, concentration and pH become a determinant of the level of homogeneity and solubility. However, at pH 8.0 Fap1-NR$_\alpha$ is monomeric up to ~300 μM but reversibly self-associates at higher concentrations, whist at pH 5.0 it is monomeric up to ~200 μM where it then precipitates and cannot be concentrated any further (Supplementary Fig. 6). It is interesting that the theoretical pI of Fap1-NR$_\alpha$ is ~4.7 and as such after fermentation of sugars in the oral cavity and the subsequent drop in pH, in addition to the activation of the non-repeat region, the helical domain will have a net zero charge which could promote inter-domain adhesion, a property that can promote bacterial biofilm formation.

To determine whether the pH-dependent changes in Fap1 which mediate bacterial adhesion may also have an impact on *S. parasanguinis* biofilms, the level of biofilm formation under different pH conditions was examined. An increase in biofilm mass is clearly correlated with a decrease in pH of the growth media (Fig. 3A) and this suggests that pH-dependent changes are critical for biofilm formation. This led us to examine the array of Fap1-NR$_\alpha$ in the crystal lattice as this might suggest a pattern of domain interactions which are manifested within the Fap1 arrangement in oral biofilms.

Using the PISA server [33] the arrangement of Fap1-NR$_\alpha$ in the crystal lattice was tested for higher oligomeric states and resulted in the identification of two highly stable tetramers (Supplementary Fig. 7). Further, these two oligomers are interrelated and as such they represent the possibility of an infinite projection of these tetramers (Fig. 3B). We superimposed the SAXS envelope at pH 5.0 along with the β-domain based on our docking experiments described earlier (Fig. 3C and Supplementary Fig. 8). This arrangement of the α-domains represents a highly satisfactory model for biofilm interactions via this region. The host ligand binding groove of the non-repeat region, including those residues identified to play an important role in host adhesion; namely I134, E138, D142, L163, V164, I291, L292, L300, L385, N403, Q405 and I411 [14] are generally still accessible. Although not all, some Fap1 molecules would still be able to play a role in both host recognition and providing inter-bacterial aggregation.

4. Discussion

The Gram-positive SRR fimbriae are a novel family of proteins with the majority of their sequence composed of heavily glycosylated dipeptide repeats which are used to project their unique adhesins away from the bacterial surface [14]. The adhesive region of GspB from the pathogen *Streptococcus gordonii* has been determined by X-ray crystallography and is very different to that of Fap1-NR, which reflects the plethora of receptors which this family recognize [34]. *S. parasanguinis* has evolved mechanisms to in-

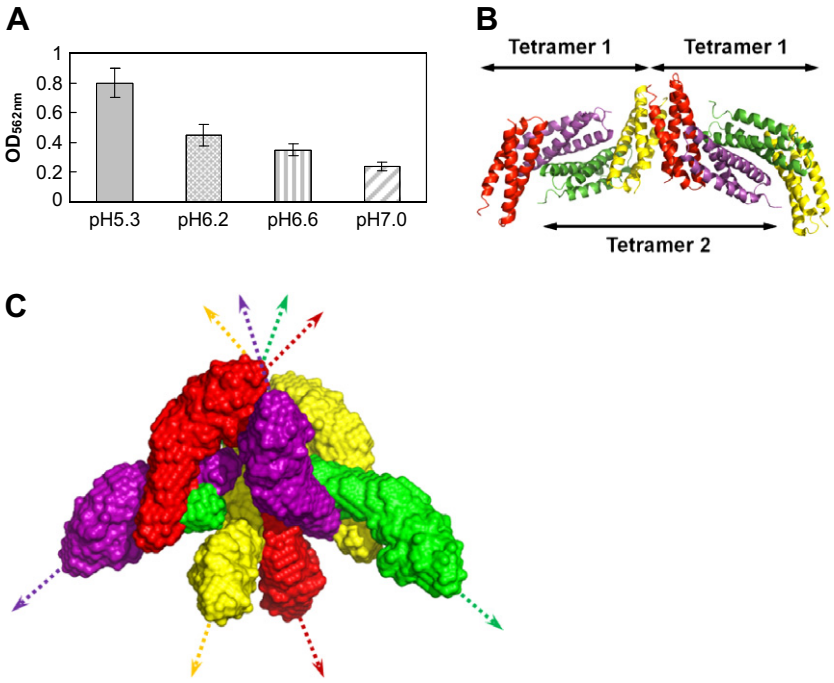

Fig. 3. Atomic model of inter-Fap1-NR interactions within oral biofilms. (A) Biofilm formation of *S. parasanguinis* under different pH conditions. Values are the means and standard deviations from three independent experiments. (B) Two stable tetramers of Fap1-NR_α which form within the crystals are shown coloured as in Fig. 1B. The two tetramers are interrelated giving rise to higher oligomeric states. (C) Model of inter-Fap1 interactions within a biofilm. The SAXS envelopes of Fap1-NR at pH 5.0 (Fig. 2D) have been docked onto the Fap1-NR_α octamer and are shown with the arrows depicting the serine-rich repeat regions pointing towards their C-termini and the bacterial cell wall. Although the tips of Fap1-NR_α interact within this array of molecules, the Fap1 host binding site is still accessible.

crease its fitness within an ever fluctuating environment and our results present the first atomic details of how pH is used to regulate the adhesive properties of Fap1 in orchestrating one of these processes. The recent crystal structure of the *Euprosthenops australis* spidroin N-terminal domain [35] has detailed how self-assembly of spider silk is also coordinated by an electrostatic switch and further shows how reorganization of protein–protein interactions via pH-induced changes in charge distribution can lead to dramatic remodelling of macromolecular structures. In addition, electrostatic potential has been shown to modulate the enzyme activity of cellobiohydrolase I from the fungus *Trichoderma reesei* [36]. Whilst the specific receptor for Fap1 still remains elusive, it is now clear how pH is used to prime the adhesive region for host and inter-fimbrial interactions under acidic conditions.

Acknowledgments

The authors would like to thank the Wellcome Trust and the beamline scientists at PXIII of the Swiss Light Source.

Appendix A. Supplementary data

Supplementary data associated with this article can be found, in the online version, at doi:10.1016/j.bbrc.2011.11.131.

References

[1] M.R. Becker, B.J. Paster, E.J. Leys, M.L. Moeschberger, S.G. Kenyon, J.L. Galvin, S.K. Boches, F.E. Dewhirst, A.L. Griffen, Molecular analysis of bacterial species associated with childhood caries, Journal of clinical microbiology 40 (2002) 1001–1009.
[2] S. Paju, F.A. Scannapieco, Oral biofilms, periodontitis, and pulmonary infections, Oral diseases 13 (2007) 508–512.
[3] F.A. Scannapieco, R.B. Bush, S. Paju, Associations between periodontal disease and risk for atherosclerosis, cardiovascular disease, and stroke. A systematic review, Annals of periodontology/the American Academy of Periodontology 8 (2003) 38-53.
[4] S. Fujitani, M.C. Rowlinson, W.L. George, Penicillin G-resistant viridans group streptococcal endocarditis and interpretation of the American Heart Association's Guidelines for the Treatment of Infective Endocarditis, Clinical infectious diseases: an official publication of the Infectious Diseases Society of America 46 (2008) 1064–1066.
[5] E. Giannitsioti, C. Chirouze, A. Bouvet, I. Beguinot, F. Delahaye, J.L. Mainardi, M. Celard, L. Mihaila-Amrouche, V.L. Moing, B. Hoen, Characteristics and regional variations of group D streptococcal endocarditis in France, Clinical microbiology and infection: the official publication of the European Society of Clinical Microbiology and Infectious Diseases 13 (2007) 770–776.
[6] K. Westling, I. Julander, P. Ljungman, S. Jalal, C.E. Nord, B. Wretlind, Viridans group streptococci in blood culture isolates in a Swedish university hospital: antibiotic susceptibility and identification of erythromycin resistance genes, International journal of antimicrobial agents 28 (2006) 292–296.
[7] P.E. Kolenbrander, Oral microbial communities: biofilms, interactions, and genetic systems, Annual Review of Microbiology 54 (2000) 413–437.
[8] J.W. Costerton, Z. Lewandowski, D.E. Caldwell, D.R. Korber, H.M. Lappin-Scott, Microbial biofilms, Annual review of microbiology 49 (1995) 711–745.
[9] H. Wu, K.P. Mintz, M. Ladha, P.M. Fives-Taylor, Isolation and characterization of Fap1, a fimbriae-associated adhesin of *Streptococcus parasanguis* FW213, Molecular Microbiology 28 (1998) 487–500.
[10] H. Wu, P.M. Fives-Taylor, Identification of dipeptide repeats and a cell wall sorting signal in the fimbriae-associated adhesin, Fap1, of *Streptococcus parasanguis*, Molecular microbiology 34 (1999) 1070–1081.
[11] A.E. Stephenson, H. Wu, J. Novak, M. Tomana, K. Mintz, P. Fives-Taylor, The Fap1 fimbrial adhesin is a glycoprotein: antibodies specific for the glycan moiety block the adhesion of *Streptococcus parasanguis* in an in vitro tooth model, Molecular microbiology 43 (2002) 147–157.
[12] M. Zhou, H. Wu, Glycosylation and biogenesis of a family of serine-rich bacterial adhesins, Microbiology 155 (2009) 317–327.
[13] E.H. Froeliger, P. Fives-Taylor, *Streptococcus parasanguis* fimbria-associated adhesin fap1 is required for biofilm formation, Infection and immunity 69 (2001) 2512–2519.
[14] S. Ramboarina, J.A. Garnett, M. Zhou, Y. Li, Z. Peng, J.D. Taylor, W.C. Lee, A. Bodey, J.W. Murray, Y. Alguel, J. Bergeron, B. Bardiaux, E. Sawyer, R. Isaacson, C. Tagliaferri, E. Cota, M. Nilges, P. Simpson, T. Ruiz, H. Wu, S. Matthews, Structural insights into serine-rich fimbriae from Gram-positive bacteria, Journal of Biological Chemistry 285 (2010) 32446–32457.
[15] K. Igarashi, K. Kamiyama, T. Yamada, Measurement of pH in human dental plaque in vivo with an ion-sensitive transistor electrode, Archives of oral biology 26 (1981) 203–207.
[16] J. Welin-Neilands, G. Svensater, Acid tolerance of biofilm cells of Streptococcus mutans, Applied and environmental microbiology 73 (2007) 5633–5638.
[17] K. McNeill, I.R. Hamilton, Acid tolerance response of biofilm cells of Streptococcus mutans, FEMS microbiology letters 221 (2003) 25–30.

[18] G. Svensater, U.B. Larsson, E.C. Greif, D.G. Cvitkovitch, I.R. Hamilton, Acid tolerance response and survival by oral bacteria, Oral microbiology and immunology 12 (1997) 266–273.

[19] J.A. Garnett, S. Ramboarina, W.C. Lee, C. Tagliaferri, W. Wu, S. Matthews, Crystallization and initial crystallographic analysis of the Streptococcus parasanguinis FW213 Fap1-NRalpha adhesive domain at pH 5.0, Acta Crystallogr Sect F Structural Biology and Crystallization Communications 67 274–276.

[20] A.G. Leslie, The integration of macromolecular diffraction data, Acta Crystallogr. D Biol. Crystallogr. 62 (2006) 48–57.

[21] P. Evans, Scaling and assessment of data quality, Acta Crystallogr. D Biol. Crystallogr. 62 (2006) 72–82.

[22] A. Vagin, A. Teplyakov, Molecular replacement with MOLREP, Acta Crystallographica, Section D: Biological Crystallography 66 (2010) 22–25.

[23] K. Cowtan, Recent developments in classical density modification, Acta Crystallographica, Section D: Biological Crystallography. 66 (2010) 470–478.

[24] K. Cowtan, The Buccaneer software for automated model building. 1. Tracing protein chains, Acta Crystallogr. D Biol. Crystallogr. 62 (2006) 1002–1011.

[25] G.N. Murshudov, A.A. Vagin, E.J. Dodson, Refinement of macromolecular structures by the maximum-likelihood method, Acta Crystallogr. D Biol. Crystallogr. 53 (1997) 240–255.

[26] P. Emsley, K. Cowtan, Coot: model-building tools for molecular graphics, Acta Crystallogr. D Biol. Crystallogr. 60 (2004) 2126–2132.

[27] I.W. Davis, A. Leaver-Fay, V.B. Chen, J.N. Block, G.J. Kapral, X. Wang, L.W. Murray, W.B. Arendall 3rd, J. Snoeyink, J.S. Richardson, D.C. Richardson, MolProbity: all-atom contacts and structure validation for proteins and nucleic acids, Nucleic Acids Research 35 (2007) W375–383.

[28] G.A. O'Toole, R. Kolter, Initiation of biofilm formation in Pseudomonas fluorescens WCS365 proceeds via multiple, convergent signalling pathways: a genetic analysis, Molecular microbiology 28 (1998) 449–461.

[29] C.A. Castaneda, C.A. Fitch, A. Majumdar, V. Khangulov, J.L. Schlessman, B.E. Garcia-Moreno, Molecular determinants of the pKa values of Asp and Glu residues in staphylococcal nuclease, Proteins 77 (2009) 570–588.

[30] A. Karshikoff, V. Spassov, S.W. Cowan, R. Ladenstein, T. Schirmer, Electrostatic properties of two porin channels from Escherichia coli, Journal of molecular biology 240 (1994) 372–384.

[31] C.N. Pace, G.R. Grimsley, J.M. Scholtz, Protein ionizable groups: p*K* values and their contribution to protein stability and solubility, The Journal of biological chemistry 284 (2009) 13285–13289.

[32] M.M. Flocco, S.L. Mowbray, Strange bedfellows: interactions between acidic side-chains in proteins, Journal of molecular biology 254 (1995) 96–105.

[33] E. Krissinel, Crystal contacts as nature's docking solutions, Journal of Computational Chemistry 31 (2010) 133–143.

[34] T.M. Pyburn, B.A. Bensing, Y.Q. Xiong, B.J. Melancon, T.M. Tomasiak, N.J. Ward, V. Yankovskaya, K.M. Oliver, G. Cecchini, G.A. Sulikowski, M.J. Tyska, P.M. Sullam, T.M. Iverson, A Structural Model for Binding of the Serine-Rich Repeat Adhesin GspB to Host Carbohydrate Receptors, PLoS pathogens 7 (2011) e1002112.

[35] G. Askarieh, M. Hedhammar, K. Nordling, A. Saenz, C. Casals, A. Rising, J. Johansson, S.D. Knight, Self-assembly of spider silk proteins is controlled by a pH-sensitive relay, Nature 465 (2010) 236–238.

[36] S.V. Pingali, H.M. O'Neill, J. McGaughey, V.S. Urban, C.S. Rempe, L. Petridis, J.C. Smith, B.R. Evans, W.T. Heller, Small Angle Neutron Scattering Reveals pH-dependent Conformational Changes in *Trichoderma reesei* Cellobiohydrolase I: implications for enzymatic activity, The Journal of biological chemistry 286 (2011) 32801–32809.